Physics of Fluids

Acoustic radiation force on a free elastic sphere in a viscous fluid: Theory and experiments

Cite as: Phys. Fluids **33**, 047107 (2021); https://doi.org/10.1063/5.0041249
Submitted: 21 December 2020 . Accepted: 23 March 2021 . Published Online: 12 April 2021

Yupei Qiao (乔玉配), **Menyang Gong** (宫门阳), **Haibin Wang** (汪海宾), **Jun Lan** (蓝君), **Teng Liu** (刘腾), **Jiehui Liu** (刘杰惠), **Yiwei Mao** (毛一葳), **Aijun He** (何爱军), and **Xiaozhou Liu** (刘晓宙)

Physics of Fluids ARTICLE scitation.org/journal/phf

Acoustic radiation force on a free elastic sphere in a viscous fluid: Theory and experiments

Cite as: Phys. Fluids 33, 047107 (2021); doi: 10.1063/5.0041249
Submitted: 21 December 2020 · Accepted: 23 March 2021 ·
Published Online: 12 April 2021

Yupei Qiao (乔玉配),[1] Menyang Gong (宫门阳),[1] Haibin Wang (汪海宾),[2] Jun Lan (蓝君),[3] Teng Liu (刘腾),[1] Jiehui Liu (刘杰惠),[1] Yiwei Mao (毛一葳),[1] Aijun He (何爱军),[4] and Xiaozhou Liu (刘晓宙)[1,5,a)]

AFFILIATIONS

[1]Key Laboratory of Modern Acoustics, Collaborative Innovation Center of Advanced Microstructures, Institute of Acoustics and School of Physics, Nanjing University, Nanjing 210093, China
[2]School of Science, Jiangsu University of Science and Technology, Zhenjiang 212003, China
[3]College of Computer Science and Technology, Nanjing Tech University, Nanjing 211800, China
[4]School of Electronic Science and Engineering, Nanjing University, Nanjing 210023, China
[5]State Key Laboratory of Acoustics, Institute of Acoustics, Chinese Academy of Sciences, Beijing 100190, China

[a)]Author to whom correspondence should be addressed: xzliu@nju.edu.cn

ABSTRACT

An expression was derived from the theory for the acoustic radiation force (ARF) acting on a free spherical particle in a viscous fluid subject to an incident plane wave. In deriving this ARF, the viscosity of the fluid, the elasticity of the particle, and the particle's state when suspended freely in the liquid were considered together. Corresponding experiments were designed and conducted. To compare the ARFs measured in experiments with those predicted by theory, a sphere made of polystyrene was taken as the target particle. Based on experimental and theoretical calculations, the effects of the incident sound pressure amplitude, the frequency of the acoustic wave, and fluid viscosity were analyzed. The analysis showed that the ARF increases with increasing pressure amplitude or dynamic viscosity. There is a series of maxima or minima in the ARF that depends on dimensionless frequency kR. Moreover, the theoretical and experimental values are in good agreement. This work provides an advanced ARF theory that is able to predict real-world behavior more accurately.

I. INTRODUCTION

Acoustic radiation force (ARF) results from a nonlinear effect of a sound field and arises from the momentum transfer between a sound field and an object. The force can be used for noncontact manipulation of particles, which has widely applied in, for example, material science, ultrasonic medicine, and biophysics.[1–6] Undoubtedly, accurate evaluations of the ARFs acting on particles are required to control these particles precisely. Therefore, numerous studies concerning the ARF have been performed beginning with work by King[7] and Yosioka and Kawasima,[8] most of which was focused mainly on a fixed particle in an ideal fluid.[9–21] Both King's and Yosioka and Kawasima's theories were repeatedly used or verified by experiment.[22–25] Westervelt was the first to consider the effect of viscosity on the ARF of a fixed sphere.[26] Many papers assumed that the particle is free to move, but in the limit of low-viscosity fluid.[27–29] Doinikov formulated theoretical equations describing the behavior of a sphere (filled with a viscous compressible barotropic fluid) suspended freely in a viscous fluid that provided either strong or weak dissipation.[30] Johnson *et al.* conducted experiments and compared them with available theories[8,30,31] under microgravity conditions, as well as normal gravity conditions.[32]

Whereas all these studies have their own assumptions and limits, real applications must consider both the viscosity of the fluid, the elasticity of particles and particles suspended freely in the liquid. These factors are taken into account concurrently in our study of the ARF acting on a free elastic sphere in a viscous fluid; from theory, a general expression for this ARF for this situation is derived. In deriving the ARF, the viscosity of the fluid is arbitrary. In addition, our analytical formulation of this ARF is applied to calculate the ARF acting on any free sphere in a viscous fluid and induced by a plane wave; here, the coefficients of scattering may differ depending on the material

properties involved. To compare the ARFs measured in experiments with those predicted by theory, we choose a polystyrene sphere as the particle in our experiments and simulations. The dependence of the ARF on incident sound pressure, the frequency of the acoustic wave, and the fluid viscosity for an elastic sphere in the experiments and simulations are considered.

II. THEORY

A free sphere of radius R, which is assumed to be elastic and isotropic, is placed in a viscous fluid. Choosing a Cartesian coordinate system (x, y, z) (Fig. 1), a plane wave propagates through the liquid along the positive z-axis direction. For the analysis, a spherical coordinate system (r, θ, φ) centered on the sphere is introduced.

Under the incident sound wave, the sphere experiences an ARF owing to the momentum transfer between it and the sound field. The ARF on the free sphere in viscous fluid is given by

$$\mathbf{F} = \left\langle \int\int_{s_0} \boldsymbol{\sigma} d\mathbf{S} \right\rangle, \tag{1}$$

where $\langle\rangle$ represents the time average, $\mathbf{S}$ denotes the surface of the target and the tensor of stresses $\boldsymbol{\sigma}$ given by

$$\boldsymbol{\sigma} = \left(-p_1 + \lambda' \nabla \cdot \mathbf{v}\right)\mathbf{E} + 2\mu' \mathbf{e}, \tag{2}$$

in which $\mathbf{E}$ denotes a unit tensor, $\mathbf{e} = ((\nabla \mathbf{v}) + (\nabla \mathbf{v})^T)/2$ the deformation velocity tensor—the superscript T denoting vector transposition, λ' and μ' denote the coefficients of second viscosity and dynamic viscosity, respectively, and

$$p_1 = \rho_0 \left(\frac{\lambda' + 2\mu'}{\rho_0} \Delta - \frac{\partial}{\partial t} \right) \Phi + \frac{\rho_0}{2c_0} \left(\frac{\partial \Phi}{\partial t} \right)^2 - \frac{1}{2} \rho_0 \left(\overrightarrow{\nabla \Phi} \right)^2 - \frac{\lambda' + 2\mu'}{c_0^2} \frac{\partial \Phi}{\partial t} \Delta \Phi, \tag{3}$$

where ρ_0 and c_0 are the density and speed of sound in viscous liquid, respectively, and the partial derivative $\partial\Phi/\partial t$ for a free object is calculated from

$$\frac{\partial \Phi}{\partial t} = \frac{d\Phi}{dt} - \mathbf{U} \cdot \nabla \Phi. \tag{4}$$

Here, $\partial\Phi/\partial t$ should be calculated in a fixed coordinate system relative to which the velocity potential is determined. The velocity vector $\mathbf{U}$ of the object is obtained from the dynamical equation

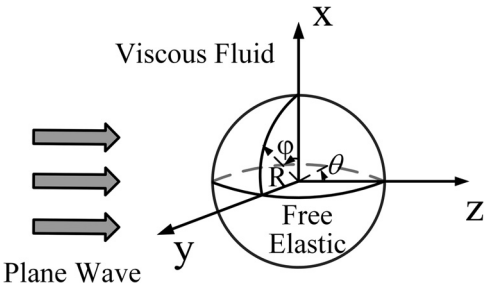

FIG. 1. Geometrical configuration of a free sphere induced by a plane wave in a viscous fluid.

$$m\dot{\mathbf{U}} = \int\int_{s_0} \boldsymbol{\sigma} d\mathbf{S}, \tag{5}$$

where $m = 4\pi R^3 \rho_1/3$ yields the mass for a sphere of radius R and density ρ_1; the velocity vector $\mathbf{v}$ of the fluid is given by

$$\mathbf{v} = \nabla \Phi + \nabla \times \boldsymbol{\Psi}, \tag{6}$$

where Φ and $\boldsymbol{\Psi}$ denote the scalar and vector velocity potentials outside the sphere. Because of the symmetry of the plane wave field, the vector potential $\boldsymbol{\Psi}$ has only a nonzero φ component and is written in the form $\boldsymbol{\Psi} = (0, 0, \Psi_s)$, Ψ_s being a scalar. The total potentials Φ and Ψ outside the sphere are calculated from

$$\Phi = \Phi_{\text{inc}} + \Phi_s, \tag{7}$$

$$\Psi = \Psi_s. \tag{8}$$

The velocity potential Φ_{inc} for a plane wave is

$$\Phi_{\text{inc}} = A e^{i(\alpha z - \omega t)}, \tag{9}$$

where A denotes the amplitude, $\alpha = (\omega/c_0)[1 - i\omega(\lambda' + 2\mu')/\rho_0 c_0^2]^{-1/2}$ the complex wavenumber of longitudinal wave, ω the angular frequency, t the time, The incident plane wave can be expanded using spherical wave functions in spherical coordinates as

$$\Phi_{\text{inc}} = \sum_{n=0}^{\infty} A(2n+1) i^n j_n(\alpha r) P_n(\cos\theta) e^{-i\omega t}, \tag{10}$$

where $j_n(\cdot)$ denotes the spherical Bessel function of order n, and $P_n(\cos\theta)$ the Legendre polynomials of degree n. The velocity potentials Φ_s and Ψ_s satisfy

$$\left[\left(1 + \frac{\lambda' + 2\mu'}{c_0^2 \rho_0} \frac{\partial}{\partial t} \right) \Delta - \frac{1}{c_0^2} \frac{\partial^2}{\partial t^2} \right] \Phi_s = 0, \tag{11}$$

$$\left(\nu \Delta - \frac{\partial}{\partial t} \right) \Psi_s = 0, \; \nu = \frac{\mu'}{\rho_0}, \tag{12}$$

where ν is the coefficient of kinematic viscosity. The solutions of Eqs. (11) and (12) are written in spherical coordinates as

$$\Phi_s = \sum_{n=0}^{\infty} A_n (2n+1) i^n h_n^{(1)}(\alpha r) P_n(\cos\theta) e^{-i\omega t}, \tag{13}$$

$$\Psi_s = \sum_{n=0}^{\infty} B_n (2n+1) i^n h_n^{(1)}(\beta r) \frac{d}{d\theta} P_n(\cos\theta) e^{-i\omega t}, \tag{14}$$

where $h_n^{(1)}(\cdot)$ denotes the nth-order spherical Hankel function of the first kind, $\beta = (1+i)/\delta$ $(\delta = \sqrt{2\mu'/\rho_0\omega})$ the wavenumber of the shear wave, δ the depth of penetration of the viscous wave, and A_n and B_n denote the coefficients of scattering determined by the boundary conditions at the interface between the free elastic sphere and viscous fluid, i.e.,

$$\begin{aligned} \mathbf{v}|_{r=R} &= \bar{\mathbf{v}}|_{r=R}, \\ \boldsymbol{\sigma}|_{r=R} &= \bar{\boldsymbol{\sigma}}|_{r=R} \end{aligned} \tag{15}$$

with $\bar{\mathbf{v}}$ and $\bar{\boldsymbol{\sigma}}$ denoting the velocity vector and tensor of stresses inside the free, elastic, and isotropic sphere. In spherical coordinates, Eq. (15) takes the form

$$\begin{aligned} v_r|_{r=R} &= \bar{v}_r|_{r=R}, \\ v_\theta|_{r=R} &= \bar{v}_\theta|_{r=R}, \\ \sigma_{rr}|_{r=R} &= \bar{\sigma}_{rr}|_{r=R}, \\ \sigma_{r\theta}|_{r=R} &= \bar{\sigma}_{r\theta}|_{r=R}, \end{aligned} \tag{16}$$

where

$$v_r = \frac{\partial \Phi}{\partial r} + \frac{1}{r\sin\theta}\frac{\partial(\Psi_s \sin\theta)}{\partial \theta}, \quad \bar{v}_r = \frac{\partial \bar{\Phi}}{\partial r} + \frac{1}{r\sin\theta}\frac{\partial(\bar{\Psi} \sin\theta)}{\partial \theta},$$

$$v_\theta = \frac{1}{r}\frac{\partial \Phi}{\partial \theta} - \frac{1}{r}\frac{\partial(r\Psi_s)}{\partial r}, \quad \bar{v}_\theta = \frac{1}{r}\frac{\partial \bar{\Phi}}{\partial \theta} - \frac{1}{r}\frac{\partial(r\bar{\Psi})}{\partial r},$$

$$\sigma_{rr} = -p_1 + 2\mu'\frac{\partial v_r}{\partial r} + \lambda'\left(\frac{\partial v_r}{\partial r} + \frac{1}{r}\frac{\partial v_\theta}{\partial \theta} + \frac{2v_r}{r} + \frac{v_\theta \cot\theta}{r}\right),$$

$$\sigma_{r\theta} = \frac{\mu'}{r}\left(r\frac{\partial v_\theta}{\partial r} - v_\theta + \frac{\partial v_r}{\partial \theta}\right),$$

$$\bar{\sigma}_{rr} = -\lambda k_L^2 \bar{\Phi} + 2\mu\left[\frac{\partial^2}{\partial r^2}\left(\bar{\Phi} + \frac{\partial}{\partial r}(r\bar{\Psi})\right) + k_t^2(r\bar{\Psi})\right],$$

$$\bar{\sigma}_{r\theta} = \mu\left\{2\frac{\partial}{\partial r}\left[\frac{1}{r}\frac{\partial}{\partial \theta}\left(\bar{\Phi} + \frac{\partial}{\partial r}(r\bar{\Psi})\right)\right] + k_t^2\frac{\partial \bar{\Psi}}{\partial \theta}\right\},$$

in which $k_L = \omega/c_L$ and $k_t = \omega/c_t$ are the longitudinal and transverse wavenumbers, $c_L = \sqrt{(\lambda + 2\mu)/\rho}$ and $c_t = \sqrt{\mu/\rho}$ the longitudinal and transverse wave speeds, λ and μ the Lamé constants, $\bar{\Phi}$ and $\bar{\Psi}$ the velocity potentials of the longitudinal and transverse waves inside the sphere which in spherical coordinates are

$$\bar{\Phi} = \sum_{n=0}^{\infty} \bar{A}_n (2n+1) i^n j_n(k_L r) P_n(\cos\theta) e^{-i\omega t}, \tag{17}$$

$$\bar{\Psi} = \sum_{n=0}^{\infty} \bar{B}_n (2n+1) i^n j_n(k_t r) \frac{d}{d\theta} P_n(\cos\theta) e^{-i\omega t}, \tag{18}$$

where $\bar{A}_n$ and $\bar{B}_n$ denote unknown coefficients of scattering that are also obtained by solving Eq. (16).

Substituting Eqs. (3), (7), (8), (10), (13), (14), (17), and (18) into Eq. (16), we obtain

$$\begin{pmatrix} a_{rn} & b_{rn} & \bar{a}_{rn} & \bar{b}_{rn} \\ a_{tn} & b_{tn} & \bar{a}_{tn} & \bar{b}_{tn} \\ A_{rn} & B_{rn} & \bar{A}_{rn} & \bar{B}_{rn} \\ A_{tn} & B_{tn} & \bar{A}_{tn} & \bar{B}_{tn} \end{pmatrix} \begin{pmatrix} A_n \\ B_n \\ \bar{A}_n \\ \bar{B}_n \end{pmatrix} = \begin{pmatrix} c_{rn} \\ c_{tn} \\ C_{rn} \\ C_{tn} \end{pmatrix}. \tag{19}$$

Detailed expressions for these equations are given in Appendix A. The unknown coefficients of scattering are computed by solving Eq. (19).

Substituting the coefficients of scattering (A_n and B_n) computed by solving Eq. (19) into Eqs. (7) and (8) yields the potentials (Φ and Ψ) outside the sphere and for the calculation of the ARF, we express them as

$$\Phi = \Phi_{inc} + \Phi_s = \sum_{n=0}^{\infty} (G_n + iL_n) P_n(\cos\theta) e^{-i\omega t}, \tag{20}$$

$$\Psi = \Psi_s = \sum_{n=0}^{\infty} (M_n + iN_n) \frac{d}{d\theta} P_n(\cos\theta) e^{-i\omega t}, \tag{21}$$

where

$$\begin{aligned} G_n &= \mathrm{Re}\{[Aj_n(\alpha r) + A_n h_n(\alpha r)](2n+1) i^n\}, \\ L_n &= \mathrm{Im}\{[Aj_n(\alpha r) + A_n h_n(\alpha r)](2n+1) i^n\}, \\ M_n &= \mathrm{Re}\{B_n h_n(\beta r)(2n+1) i^n\}, \\ N_n &= \mathrm{Im}\{B_n h_n(\beta r)(2n+1) i^n\}. \end{aligned}$$

By incorporating Eqs. (2)–(6), (20), and (21) into Eq. (1), we obtain the ARF for a free sphere induced by a plane wave in a viscous fluid,

$$\begin{aligned} \mathrm{F} = &-6\eta\rho_0\pi\left\{\frac{1}{3}\left[(2N_1 - L_1)G_0 + (G_1 - 2M_1)L_0\right]\right. \\ &\left. + \frac{2}{5}\left[(2N_1 - L_1)G_2 + (G_1 - 2M_1)L_2\right]\right\} \\ &- \pi\rho_0\left(\frac{\omega R}{c_0}\right)^2 \sum_{n=0}^{\infty} \frac{n+1}{(2n+1)(2n+3)}(G_n G_{n+1} + L_n L_{n+1}) \\ &+ \pi\rho_0 \sum_{n=0}^{\infty} \frac{n(n+2)(n+1)}{(2n+1)(2n+3)}\left[(n+1)^2(M_n M_{n+1} + N_n N_{n+1})\right. \\ &\left. + (G_n G_{n+1} + L_n L_{n+1})\right] + \frac{2\pi R^2(\lambda' + 2\mu')\rho_0\omega^3}{\rho_0^2 c_0^2 + \omega^2(\lambda' + 2\mu')^2} \\ &\times \sum_{n=0}^{\infty} \frac{n+1}{(2n+1)(2n+3)}\begin{bmatrix} \rho_0(G_n L_{n+1} - L_n G_{n+1}) \\ +(\lambda' + 2\mu')\omega(G_n G_{n+1} + L_n L_{n+1}) \end{bmatrix}. \end{aligned} \tag{22}$$

Note that F given in Eq. (22) is the ARF of the sphere along the z-axis direction, and also its resultant force. Because of the symmetry of the plane wave field, the resultant ARF on the sphere is along the z-axis direction. The expression of F is applicable for any viscous fluid in which plane waves propagate and any sphere regardless of composition. The various coefficients of scattering differ depending on the material of the sphere and therefore Eq. (22) represents an advance regarding the derivation of the ARF.

III. EXPERIMENT

The radiation force measurements were performed in a tank of dimensions $8 \times 8 \times 20\mathrm{cm}^3$ using degassed water in which a polystyrene sphere was suspended freely [see Figs. 2(a) and 2(b) for the laboratory setup]. The tank was placed on a mobile platform and maintained at a constant temperature (27 °C) using an air conditioner to minimize the effects of thermal convection. A 2-cm-diameter transducer was mounted in the center of the $8 \times 8\mathrm{cm}^2$ wall along the z-axis (see Fig. 2). The transducer was excited in each test by a signal produced by a function generator (Agilent, 33250A), the signal being amplified by a power amplifier. A sound absorption material was positioned in front of the opposite wall to that of the transducer to permit the particle to move without restrictions imposed by physical boundaries. The experimental device (including tank, microscope, and mobile platform) was placed on a shockproof platform to reduce tank vibrations caused by the surrounding environment. The movement of the particle was observed using a microscope (Olympus, SZX7) positioned above the tank and equipped with a camera (Fly, CU3E630SP), which was connected to a personal computer controlled by FlyView software. The movement of the particle was recorded in a 3072 $\times$2048 pixel^2 field with a time resolution of 1/30 s.

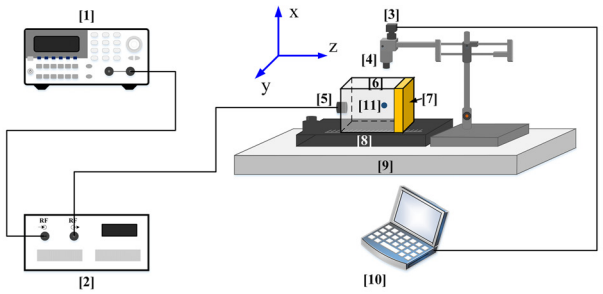

[1] Function Generator [2] Power Amplifier [3] Camera [4] Microscope
[5] Transducer [6] Water Tank [7] Sound Absorbing Material
[8] Mobile Platform [9] Shockproof Platform [10] Computer [11] Sphere

(a)

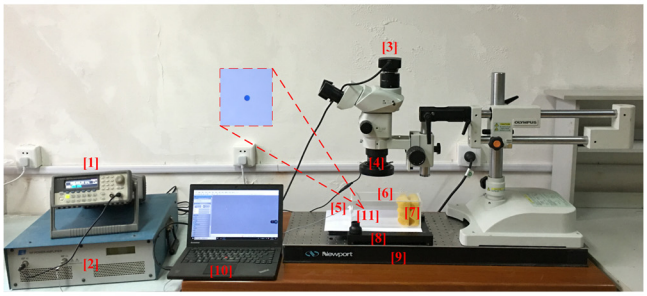

[1] Function Generator [2] Power Amplifier [3] Camera [4] Microscope
[5] Transducer [6] Water Tank [7] Sound Absorbing Material
[8] Mobile Platform [9] Shockproof Platform [10] Computer [11] Sphere

(b)

FIG. 2. (a) Schematic diagram of the experimental system. (b) Laboratory setup for ARF measurement.

A viscous liquid with the same density as polystyrene was prepared in which to suspend the sphere. Hence, gravity (G_m) and buoyancy (F_b) of the particle are balanced (see Fig. 3). We positioned the particle and the center of the transducer at the same depth so that in the theoretical analysis the acoustic field can be suitably compared to a traveling plane wave. The particle began to accelerate in the yz-plane (see Fig. 2) when the generator was turned on and subjected to the net force comprising the ARF (F) and viscous drag (F_{Drag}). Ultimately, the particle reaches a terminal velocity when the net force vanishes, indicating that the ARF and drag are equal in magnitude. Measurements were taken under this equilibrium condition, which

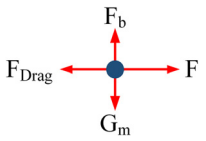

FIG. 3. Schematic diagram of forces on the spherical particle in the sound field.

permits the use of the drag (F_{Drag}) as an estimate of the ARF. Because the Reynolds numbers for the experiments conducted herein are less than two (see Tables I–III), the drag on the sphere is considered as Oseen drag.[35,36] The magnitude of the Oseen drag is

$$F_{Drag} = \frac{1}{2}\rho_0 v_{sphere}^2 \pi R^2 C_D, \tag{23}$$

where $C_D = 24/\mathrm{Re}(1 + 3\mathrm{Re}/16)$ is the drag coefficient of a free sphere,[36] and Reynolds number $\mathrm{Re} = 2R\rho_0 v_{sphere}/\mu'$ with v_{sphere} being the velocity of the sphere. Using the open-source software FIJI (IMAGEJ) with the plugin TrackMate, recorded videos of the particle moving at constant velocity were processed to extract the velocities of the particle.[33,34] The velocity data provide the input to calculate the magnitude of the Oseen drag [Eq. (23)] and thus an estimate of the ARF.

Three experiments were conducted to reveal the dependence of the ARF for the polystyrene sphere on the excitation signal amplitude, transducer frequency, and the fluid viscosity. The diameter of the sphere is (0.600 ± 0.008) mm, obtained by calculating the mean of many measurements and hence the standard deviation (SD). In the experiment with various fixed excitation signal voltages (20, 25, 30, 35, and 40 mV), the fluid was degassed salt water (dynamic viscosity, $\mu' = 0.97\mathrm{mPa}\cdot\mathrm{s}$). To reduce the effect of impurities, the salt water was produced by dissolving refined salt in purified water. The fluid viscosity was measured using a viscometer (NDJ-8S). The transducer frequency was 0.968 MHz. In the experiment in which the transducer frequency was varied, the fluid was still salt water (dynamic viscosity, $\mu' = 0.97\mathrm{mPa}\cdot\mathrm{s}$). The driving frequency was set to the center frequency of several transducers (specifically, 0.506, 0.968, 1.40, 1.98, and 2.32 MHz), as well as some values around the center frequencies. The excitation signal voltage amplitude was fixed at 20 mV. In the experiment for which the fluid viscosity varied (0.97, 1.19, 1.31, 1.52, 1.84, 2.07, 2.27, 2.58, and $2.72\mathrm{mPa}\cdot\mathrm{s}$), whereas the excitation signal voltage amplitude and the transducer frequency were fixed at 25 mV and 0.968 MHz. The dynamic viscosity of the fluid was increased by dissolving different amounts of carboxymethyl cellulose (CMC) in salt water. The CMC is a good tackifier that does not change the density of the liquid and is resistant to salt. For each of the three experiments, the pressure amplitude of the signal was measured using the calibrated needle hydrophone (ZS-1000) to compare the measured ARF with that predicted by theory quantitatively.

TABLE I. The pressure amplitudes (p), velocities (v_{sphere}), and Reynolds numbers (Re) of a 0.600 mm-diameter polystyrene sphere in degassed salt water ($\mu' = 0.97$ mPa s) at different input voltage amplitudes when the transducer frequency is 0.968 MHz. The p, v_{sphere}, and Re are in the form of average values and SDs.

Voltage amplitudes	p (kPa)	v_{sphere} (mm/s)	Re
20 mV	21.680 ± 1.227	0.211 ± 0.031	0.13 ± 0.02
25 mV	24.834 ± 0.415	0.274 ± 0.014	0.17 ± 0.01
30 mV	26.679 ± 0.808	0.309 ± 0.025	0.19 ± 0.02
35 mV	29.861 ± 2.045	0.380 ± 0.029	0.23 ± 0.02
40 mV	31.357 ± 1.699	0.409 ± 0.011	0.25 ± 0.01

TABLE II. The kR, velocities (v_{sphere}), and Reynolds numbers (Re) of a 0.600 mm-diameter polystyrene sphere in degassed salt water ($\mu' = 0.97$ mPa s) at different frequencies (f) when the input voltage amplitude is 20 mV. The v_{sphere} and Re are in the form of average values and SDs.

f (MHz)	kR	v_{sphere} (mm/s)	Re
0.506	0.636	0.014 ± 0.001	0.01 ± 0.00
0.910	1.14	0.184 ± 0.003	0.11 ± 0.00
0.918	1.15	0.359 ± 0.028	0.22 ± 0.02
0.923	1.16	0.549 ± 0.007	0.34 ± 0.01
0.950	1.19	0.380 ± 0.029	0.23 ± 0.02
0.968	1.22	0.211 ± 0.031	0.13 ± 0.02
1.40	1.76	0.488 ± 0.084	0.30 ± 0.01
1.42	1.78	0.543 ± 0.039	0.33 ± 0.03
1.47	1.85	0.640 ± 0.002	0.39 ± 0.01
1.52	1.91	0.532 ± 0.046	0.33 ± 0.03
1.85	2.32	0.218 ± 0.025	0.13 ± 0.02
1.89	2.38	0.380 ± 0.029	0.23 ± 0.02
1.93	2.43	0.304 ± 0.013	0.19 ± 0.01
1.98	2.49	0.180 ± 0.011	0.11 ± 0.01
2.32	2.92	0.032 ± 0.004	0.20 ± 0.00

From the minimum of five videos saved for each test, each video was processed using the open-source software FIJI (IMAGEJ).[33,34] Figure 4 illustrates the movement of the particle at constant velocity in degassed salt water (dynamic viscosity, $\mu' = 0.97\text{mPa} \cdot \text{s}$) at fixed transducer frequency and excitation signal voltage amplitude. The image is a time composite image of the particle's movement, which was created by compositing the frames of Figs. 8(a)–8(f) in Appendix B and show the positions of the particle in the sound field at time intervals of 4/30 s. To obtain the velocity and position of the particle in each video, the plugin TrackMate was used.[34] This plugin needs a threshold stack to properly track the particle, hence the video needed to be processed before using the tracking plugin. Details are presented in Refs. 33 and 34.

TABLE III. The velocities (v_{sphere}), and Reynolds numbers (Re) of a 0.600 mm-diameter polystyrene sphere at different dynamic viscosities (μ') when the input voltage amplitude is 25 mV and the transducer frequency is 0.968 MHz. Parameters are in the form of average values and SDs.

μ' (mPa s)	v_{sphere} (mm/s)	Re
0.97 ± 0.02	0.274 ± 0.014	0.17 ± 0.01
1.19 ± 0.00	0.286 ± 0.034	0.14 ± 0.02
1.31 ± 0.01	0.260 ± 0.014	0.12 ± 0.01
1.52 ± 0.00	0.274 ± 0.014	0.11 ± 0.01
1.84 ± 0.00	0.339 ± 0.013	0.11 ± 0.00
2.07 ± 0.02	0.316 ± 0.005	0.09 ± 0.00
2.27 ± 0.00	0.304 ± 0.013	0.08 ± 0.00
2.58 ± 0.00	0.380 ± 0.029	0.09 ± 0.01
2.72 ± 0.00	0.339 ± 0.013	0.07 ± 0.00

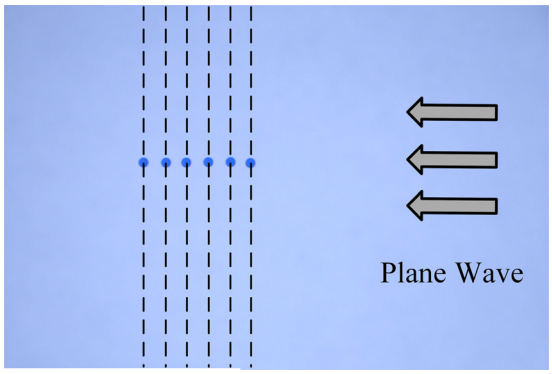

FIG. 4. A time composite image of the movement of the particle at constant velocity in degassed salt water (dynamic viscosity, $\mu' = 0.97\text{mPa} \cdot \text{s}$) at fixed transducer frequency and excitation signal voltage amplitude.

IV. RESULTS AND DISCUSSION

The ARFs obtained through experimental measurements [Eq. (23)] and from theory [Eq. (22)] were compared and analyzed. For theoretical calculation, the parameters settings for the polystyrene sphere were density $\rho_1 = 1050\text{kg/m}^3$, longitudinal compressional velocity $c_L = 2340\text{m/s}$, and compressional velocity $c_t = 1150\text{m/s}$. The density and sound velocity of the fluid were $\rho_0 = 1000\text{kg/m}^3$ and $c_0 = 1500\text{m/s}$, respectively. The transducer frequency, particle diameter, particle density, and fluid viscosity for both experiment and theory also matched.

A. Varying the incident pressure amplitude

In the first experiment with fixed transducer frequency and dynamic viscosity, various voltage amplitudes were used in producing the excitation signal. However, because the voltage amplitude is not directly used in the theoretical calculation, the pressure amplitude associated with each voltage was measured to enable a quantitative comparison of the measured ARF with theory. Table I lists the average values of the pressure amplitudes and their corresponding SDs. The average values and SDs of the velocities and corresponding Reynolds numbers of a 0.600 mm-diameter polystyrene sphere in degassed salt water are also given in Table I. Because the Reynolds numbers are less than two, the expression for Oseen drag is used. Substituting the velocities into the Oseen drag equation [Eq. (23)] yields the ARFs acting on the particle and the results are displayed in Fig. 5. The pressure dependence of the ARFs obtained from theory for the 0.600 mm-diameter polystyrene sphere in degassed salt water is also shown (dashed line in Fig. 5). The scatterplot corresponds to the experimental values with error bars indicating the SDs.

The results in Fig. 5 show that the ARF increases with increasing pressure amplitude, that is, with increasing voltage amplitude of the excitation signal. The theoretical and experimental results have a reasonable agreement. Their relative error mainly stems from two aspects: first, the material parameters (such as density and sound velocity) of the polystyrene sphere set in the theory are widely accepted and used by researchers. The polystyrene sphere used in the experiments is customized; its parameter values are as far as possible close to the theoretical parameters, but it not be completely consistent because of the

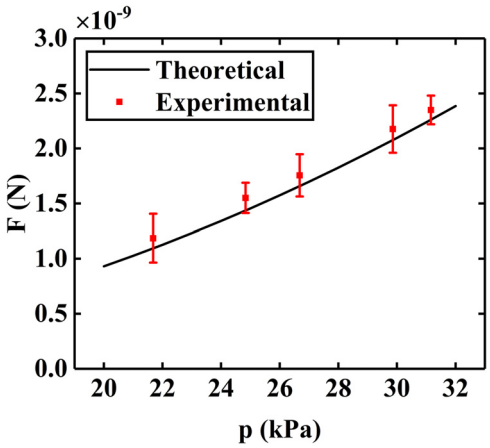

FIG. 5. ARFs vs pressure amplitude for the 0.600 mm-diameter polystyrene sphere in degassed salt water ($\mu' = 0.97$ mPa s) when the transducer frequency is 0.968 MHz. Dashed line corresponds to the theoretical values. The scatterplot corresponds to the experimental values with error bars indicating the SDs.

influence of processing errors. Second, the movement of the particle is affected by disturbances from vibrations external to the tank. For large pressure amplitudes, the experimental results are close to theoretical values because the particle passes through the microscope's field of view with large velocities, the disturbance having little effect.

B. Varying the dimensionless frequency kR

In the second experiment, the input signal voltage amplitude was set to 20 mV, which corresponds to a sound pressure amplitude of 21.680 kPa. The particle remained unchanged. The dynamic viscosity of the fluid $\mu' = 0.97\text{mPa} \cdot \text{s}$. The transducer frequency was varied over selected values listed in Table II. The corresponding $kR = 2\pi f/c_0 R$, particle velocities and Reynolds numbers including their average values and SDs are also given in Table II. The ARFs measured experimentally were obtained by substituting the velocities into Eq. (23) and the results are plotted in Fig. 6. The ARFs calculated theoretically are also presented in Fig. 6. For greater detail, the area S1 in Fig. 6(a) has been enlarged in Fig. 6(b).

In Fig. 6, the dashed line displays the theoretical value. The scatterplot displays the experimental values with SDs. The curve F − kR calculated from theory shows maxima or minima owing to the interaction between the particle and sound field, which also appears in experiments at the same kR points. There is an obvious discrepancy in the peaks between experiment and theory, which mostly stems from the energy of the sound field excited by the transducer with an off-center frequency smaller than the theoretical value. Nonetheless, the theoretical model captures similar trends as those observed in the experiments and the experimental results are of the same order of magnitude as the theoretical predictions. There are also many other factors in the experiment that cannot be captured in simple theoretical models. We thus deem the experimental results and theoretical predictions to be in reasonable agreement.

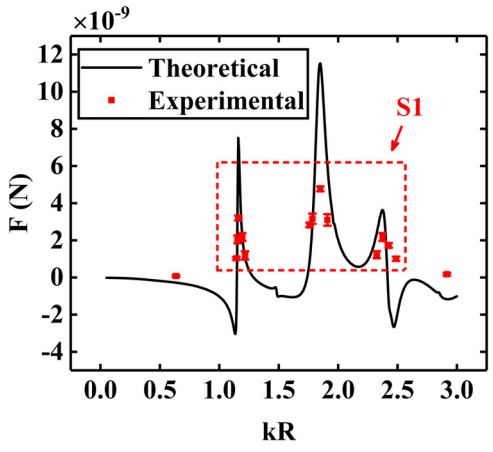

(a)

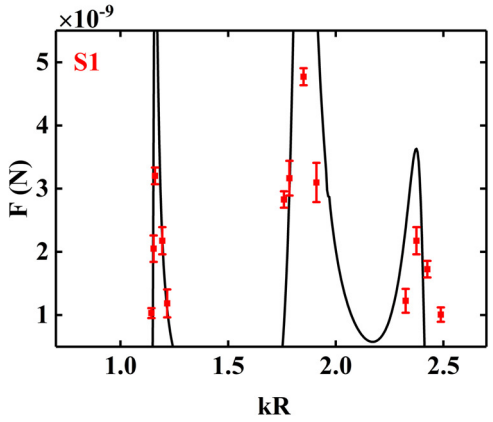

(b)

FIG. 6. ARFs vs kR for the 0.600 mm-diameter polystyrene sphere in degassed salt water ($\mu' = 0.97$ mPa s) when the input voltage amplitude is 20 mV. Dashed line corresponds to the theoretical values. The scatterplot corresponds to the experimental values with error bars indicating the SDs. (a) ARFs vs kR for the sphere, (b) enlarged view of area S1 in Fig. (a).

C. Varying the dynamic viscosity of the fluid

An experiment in which the sphere suspended freely in fluids of different viscosities was performed. The transducer frequency was set to 0.968 MHz, and the amplitude of sound pressure was fixed at 24.834 kPa corresponding to 25 mV voltage. The average values and SDs of the dynamic viscosities, particle velocities, and Reynolds numbers are listed in Table III in the form of average values and standard deviations. The fluid viscosity was measured using the viscometer. To reduce the influence of errors incurred from the viscosity measurements, the viscosity of each liquid was measured six times before and after the experiment. A comparison of the ARFs action on the polystyrene sphere measured in the experiment and calculated from theory is presented in Fig. 7. The dashed line denotes the theoretical value. The scatterplot corresponds to the experimental values and their SDs. We find the ARF increases with the increasing dynamic viscosity. Moreover, the experimental values are scattered about the theoretical

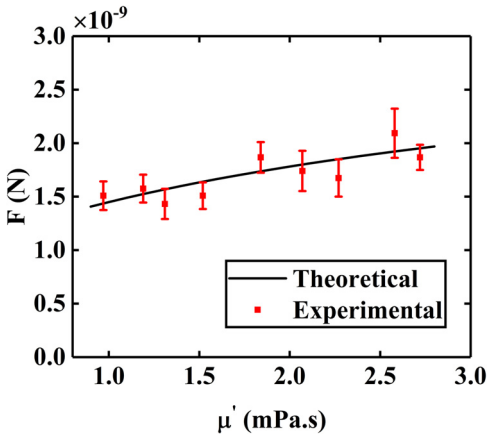

FIG. 7. ARFs vs dynamic viscosity of fluid for the 0.600 mm-diameter polystyrene sphere when the input voltage amplitude is 25 mV and the transducer frequency is 0.968 MHz. Dashed line corresponds to the theoretical values. The scatterplot corresponds to the experimental values with error bars indicating the SDs.

values. A possible explanation for the discrepancies has been stated in Sec. IV A and is applicable here. Furthermore, for $\mu' = 0.97$ mPa s as an example, the ARF measured by experiment is 1.51×10^{-9}N and that obtained from Eq. (22) is 1.44×10^{-9}N. However, for the polystyrene sphere in a nonviscous fluid, keeping all parameters fixed except the coefficient of viscosity for the liquid, the ARF calculated by the theory given in Ref. 37 is 4.70×10^{-9}N, the difference between the result and the experimental result being more than a factor 3. The ARFs obtained from the present theory [i.e., Eq. (22)] are closer to the experimental results.

V. CONCLUSIONS

For the applications of ARF in particle manipulations, accurate estimates of it are essential. An expression of the ARF for a free sphere in a viscous fluid and excited by an incident plane wave was derived. In its derivation, the viscosity of the fluid is arbitrary. We considered scenarios in which the fluid viscosity, the particle elasticity, and the state of the freely suspended particle in the liquid are taken into account simultaneously. Experiments were designed and performed to reveal the effects of pressure amplitude, acoustic frequency, and viscosity of fluid on the ARF of a free polystyrene sphere. The ARFs obtained through theory and experiment were compared. Both results showed similar trends and the same order of magnitude. The theoretical and experimental values were in reasonable agreement. This work advances the analysis of the ARF enabling more accurate estimates in real-world applications.

ACKNOWLEDGMENTS

This work was supported by National Key R & D Program of China (No. 2020YFA0211400), State Key Program of National Natural Science of China (No. 11834008), National Natural Science Foundation of China (No. 11774167), State Key Laboratory of Acoustics, Chinese Academy of Science (No. SKLA202008), Key Laboratory of Underwater Acoustic Environment, Chinese Academy of Sciences (No. SSHJ-KFKT-1701), and AQSIQ Technology R&D Program, China (No. 2017QK125).

AUTHORS' CONTRIBUTIONS

Y. Qiao and M. Gong contributed equally to this work.

APPENDIX A: THE DETAILED EXPRESSIONS OF THE EQUATIONS IN EQ. (18)

The detailed expressions of the equations in Eq. (18) as follows:

$$a_{rn} = nh_n^{(1)}(\alpha R) - \alpha R h_{n+1}^{(1)}(\alpha R),$$

$$b_{rn} = -n(n+1)h_n^{(1)}(\beta R),$$

$$\bar{a}_{rn} = k_L R j_{n+1}(k_L R) - n j_n(k_L R),$$

$$\bar{b}_{rn} = n(n+1) j_n(k_t R),$$

$$c_{rn} = -A\left[n j_n(\alpha R) - \alpha R j_{n+1}(\alpha R)\right],$$

$$a_{tn} = h_n^{(1)}(\alpha R),$$

$$b_{tn} = -n(n+1)h_n^{(1)}(\beta R) + \beta r h_{n+1}^{(1)}(\beta R),$$

$$\bar{a}_{tn} = -j_n(k_L R),$$

$$\bar{b}_{tn} = n(n+1) j_n(k_t R) - k_t R j_{n+1}(k_t R),$$

$$c_{tn} = -A j_n(\alpha R),$$

$$A_{rn} = \mu'\left[\left(n^2 - n - 0.5\beta^2 R^2\right)h_n^{(1)}(\alpha R) + 2\alpha R h_{n+1}^{(1)}(\alpha R)\right],$$

$$B_{rn} = \mu'\left[n(n+1)(1-n)h_n^{(1)}(\beta R) + n(n+1)(\beta R)h_{n+1}^{(1)}(\beta R)\right],$$

$$\bar{A}_{rn} = \mu\left[\left(-n^2 + n + k_L^2 R^2 + \frac{\lambda}{2\mu}k_L^2 R^2\right) j_n(k_L R) - k_L R j_{n+1}(k_L R)\right],$$

$$\bar{B}_{rn} = \mu\left[n(n-1)(n+1) j_n(k_t R) - n(n+1) k_t R j_{n+1}(k_t R)\right],$$

$$C_{rn} = -\mu' A\left[\left(n^2 - n - 0.5\beta^2 R^2\right) j_n(\alpha R) + 2\alpha R j_{n+1}(\alpha R)\right],$$

$$A_{tn} = \mu'\left[(n-1)h_n^{(1)}(\alpha R) - \alpha R h_{n+1}^{(1)}(\alpha R)\right],$$

$$B_{tn} = \mu'\left[\left(-n^2 + 1 + 0.5\beta^2 R^2\right)h_n^{(1)}(\beta R) - (\beta R)h_{n+1}^{(1)}(\beta R)\right],$$

$$\bar{A}_{tn} = \mu\left[(1-n) j_n(k_L R) + k_L R j_{n+1}(k_L R)\right],$$

$$\bar{B}_{tn} = \mu\left[\left(n^2 - 1 - 0.5k_t^2 R^2\right) j_n(k_t R) + k_t R j_{n+1}(k_t R)\right],$$

$$C_{tn} = -\mu' A\left[(n-1) j_n(\alpha R) - \alpha R j_{n+1}(\alpha R)\right].$$

APPENDIX B: THE POSITIONS OF THE PARTICLE IN THE SOUND FIELD AT TIME INTERVALS OF 4/30 s

Figures 8(a)–8(f) show the positions of the particle in the sound field at time intervals of 4/30 s when the particle movement at constant velocity in degassed salt water.

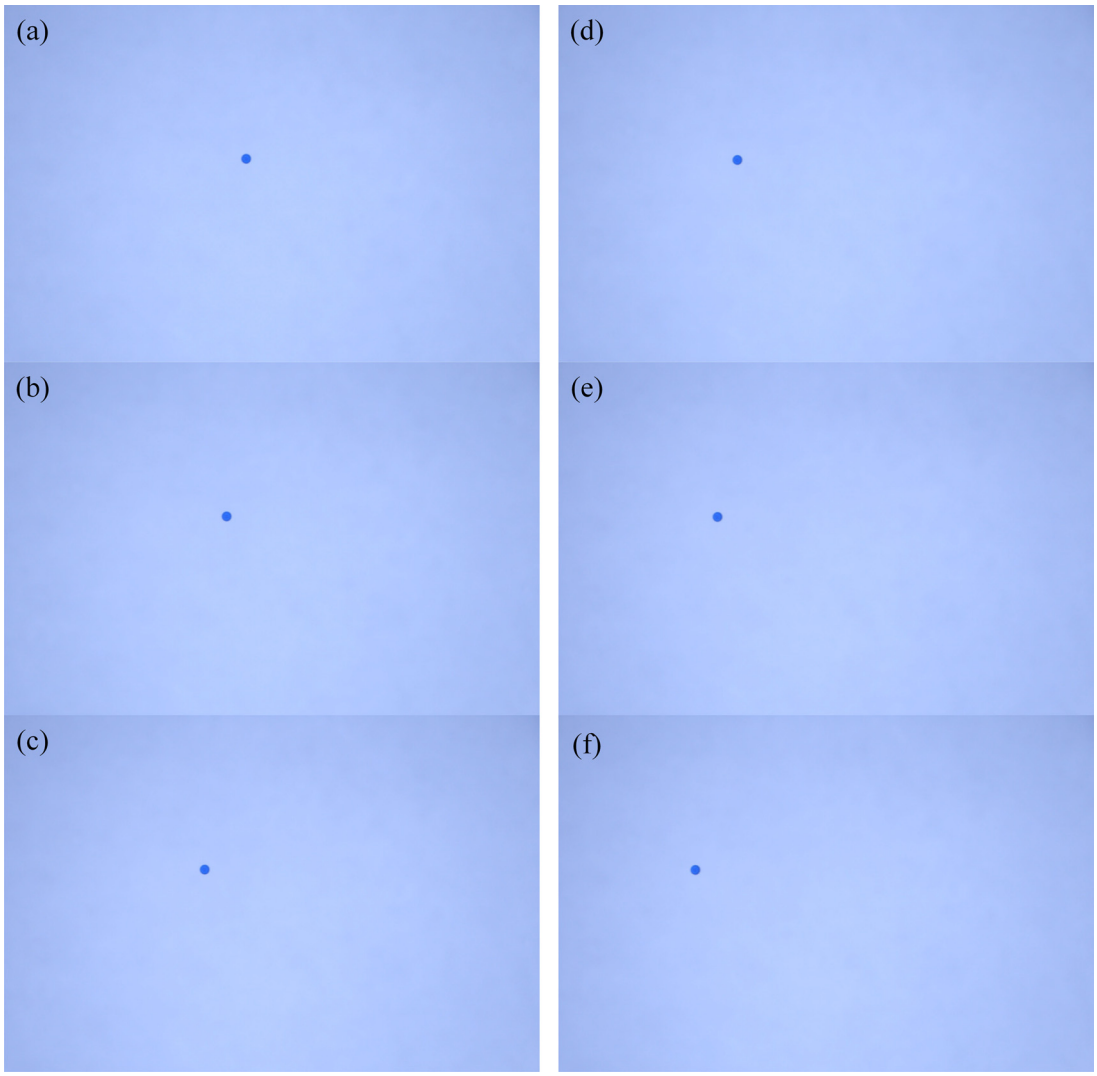

FIG. 8. Positions of the particle in the sound field at time intervals 4/30 s when the particle movement at constant velocity in degassed salt water at fixed transducer frequency and excitation signal voltage amplitude.

DATA AVAILABILITY

The data that support the findings of this study are available from the corresponding author upon reasonable request.

REFERENCES

[1]M. K. Nichols, R. K. Kumar, P. G. Bassindale, L. Tian, A. C. Barnes, B. W. Drinkwater, A. J. Patil, and S. Mann, "Fabrication of micropatterned dipeptide hydrogels by acoustic trapping of stimulus-responsive coacervate droplets," Small **14**, 1800739 (2018).
[2]L. Tian, N. Martin, P. G. Bassindale, A. J. Patil, M. Li, A. Barnes, B. W. Drinkwater, and S. Mann, "Spontaneous assembly of chemically encoded two-dimensional coacervate droplet arrays by acoustic wave patterning," Nat. Commun. **7**, 13068 (2016).
[3]J. R. Wu, "Acoustical tweezers," J. Acoust. Soc. Am. **89**, 2140–2143 (1991).
[4]A. Ozcelik, J. Rufo, F. Guo, Y. Gu, P. Li, J. Lata, and T. J. Huang, "Acoustic tweezers for the life sciences," Nat. Methods **15**, 1021–1028 (2018).
[5]M. X. Wu, P. Huang, R. Zhang *et al.*, "Circulating tumor cell phenotyping via high-throughput acoustic separation," Small **14**, 1801131 (2018).
[6]A. P. Sarvazyan, O. V. Rudenko, and W. L. Nyborg, "Biomedical applications of radiation force of ultrasound: Historical roots and physical basis," Ultrasound Med. Biol. **36**, 379–1394 (2010).
[7]L. V. King, "On the acoustic radiation pressure on sphere," Proc. R. Soc. London, Ser. A. **147**, 212–240 (1934).
[8]K. Yosioka and Y. Kawasima, "Acoustic radiation pressure on a compressible sphere," Acustica **5**, 167–173 (1955).
[9]J. R. Wu and G. H. Du, "Acoustic radiation force on a small compressible sphere in a focused beam," J. Acoust. Soc. Am. **87**, 997–1003 (1990).
[10]T. Hasegawa, K. Saka, N. Inoue, and K. Matsuzawa, "Acoustic radiation force experienced by a solid elastic cylinder in a plane progressive sound field," J. Acoust. Soc. Am. **83**, 1770–1775 (1988).

[11]Y. P. Qiao, X. F. Zhang, and G. B. Zhang, "Acoustic radiation force on a fluid cylindrical particle immersed in water near an impedance boundary," J. Acoust. Soc. Am. **141**, 4633–4641 (2017).
[12]P. L. Marston, "Axial radiation force of a Bessel beam on a sphere and direction reversal of the force," J. Acoust. Soc. Am. **120**, 3518–3524 (2006).
[13]J. Shi, S. Li, Y. Deng, X. F. Zhang, and G. B. Zhang, "Analysis of acoustic radiation force on a rigid sphere in a fluid-filled cylindrical cavity with an abruptly changed cross-section," J. Acoust. Soc. Am. **147**, 516–524 (2020).
[14]H. B. Wang, S. Gao, Y. P. Qiao, J. H. Liu, and X. Z. Liu, "Theoretical study of acoustic radiation force and torque on a pair of polymer cylindrical particles in two Airy beams fields," Phys. Fluids **31**, 047103 (2019).
[15]J. Wang and J. Dual, "Theoretical and numerical calculation of the acoustic radiation force acting on a circular rigid cylinder near a flat wall in a standing wave excitation in an ideal fluid," Ultrasonics **52**, 325–332 (2012).
[16]J. Lee, S. Y. Teh, A. Lee, H. H. Kim, C. Lee, and K. K. Shung, "Transverse acoustic trapping using a Gaussian focused beam," Ultrasound Med. Biol. **36**, 350–355 (2010).
[17]A. K. Miri and F. G. Mitri, "Acoustic radiation force on a spherical contrast agent shell near a vessel porous wall-theory," Ultrasound Med. Biol. **37**, 301–311 (2011).
[18]M. Y. Gong, Y. P. Qiao, J. Lan, and X. Z. Liu, "Far-field particle manipulation scheme based on X wave," Phys. Fluids **32**, 117104 (2020).
[19]F. G. Mitri, "Radiation forces and torque on a rigid elliptical cylinder in acoustical plane progressive and (quasi)standing waves with arbitrary incidence," Phys. Fluids **28**, 077104 (2016).
[20]P. L. Marston, "Comment on 'Radiation forces and torque on a rigid elliptical cylinder in acoustical plane progressive and (quasi)standing waves with arbitrary incidence' [Phys. Fluids **28**, 077104 (2016)]," Phys. Fluids **29**, 029101 (2017).
[21]S. Z. Hoque and A. K. Sen, "Interparticle acoustic radiation force between a pair of spherical particles in a liquid exposed to a standing bulk acoustic wave," Phys. Fluids **32**, 072004 (2020).
[22]Y. J. Wang and B. Anthony, "Characterization of wave fields using transient motion of microspheres under acoustic radiation force," Proc. Mtgs. Acoust. **34**, 030003 (2018).
[23]D. Foresti, M. Nabavi, and D. Poulikakos, "On the acoustic levitation stability behaviour of spherical and ellipsoidal particles," J. Fluid Mech. **709**, 581–592 (2012).
[24]K. Yasuda and T. Kamakura, "Acoustic radiation force on micrometer-size particles," Appl. Phys. Lett. **71**, 1771–1773 (1997).
[25]J. R. Wu, G. H. Du, S. S. Work, and D. M. Warshaw, "Acoustic radiation pressure on a rigid cylinder: An analytical theory and experiments," J. Acoust. Soc. Am. **87**, 581–586 (1990).
[26]P. J. Westervelt, "The theory of steady forces caused by sound waves," J. Acoust. Soc. Am. **23**, 312–315 (1951).
[27]A. N. Guz and A. P. Zhuk, "On the forces acting on a spherical particle in a sound field in a viscous fluid," Dokl. Akad. Nauk SSSR **274**, 1313–1316 (1984).
[28]A. N. Guz and A. P. Zhuk, "Dynamics of a rigid cylinder near a plane boundary in the radiation field of an acoustic wave," J. Fluids Struct. **25**, 1206–1212 (2009).
[29]J. Wang and J. Dual, "Theoretical and numerical calculations for the time-averaged acoustic force and torque acting on a rigid cylinder of arbitrary size in a low viscosity fluid," J. Acoust. Soc. Am. **129**, 3490–3501 (2009).
[30]A. A. Doinikov, "Acoustic radiation pressure on a compressible sphere in a viscous fluid," J. Fluid Mech. **267**, 1–21 (1994).
[31]M. Settnes and H. Bruus, "Forces acting on a small particle in an acoustical field in a viscous fluid," Phys. Rev. E **85**, 016327 (2012).
[32]K. A. Johnson, H. R. Vormohr, A. A. Doinikov *et al.*, "Experimental verification of theoretical equations for acoustic radiation force on compressible spherical particles in traveling waves," Phys. Rev. E **93**, 053109 (2016).
[33]J. Schindelin, I. Arganda-Carreras, E. Frise, V. Kaynig, M. Longair, T. Pietzsch, S. Preibisch, C. Rueden, S. Saalfeld, B. Schmid, J.-Y. Tinevez, D. J. White, V. Hartenstein, K. Eliceiri, P. Tomancak, and A. Cardona, "Fiji: An open-source platform for biological-image analysis," Nat. Methods **9**, 676–682 (2012).
[34]J. Y. Tinevez, N. Perry, J. Schindelin *et al.*, "TrackMate: An open and extensible platform for single-particle tracking," Methods **115**, 80–90 (2017).
[35]F. M. White, *Fluid Mechanics*, 8th ed. (McGraw-Hill, New York, 2015).
[36]M. V. Dyke, "Extension of Goldstein's series for the Oseen drag of a sphere," J. Fluid Mech. **44**, 365–372 (2006).
[37]T. Hasegawa and K. Yosioka, "Acoustic-radiation force on a solid elastic sphere," J. Acoust. Soc. Am. **46**, 1139–1143 (1969).